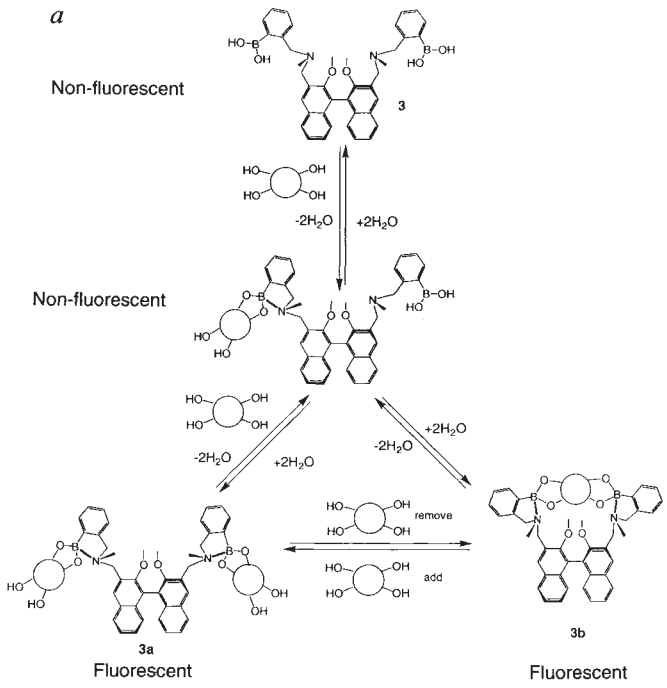

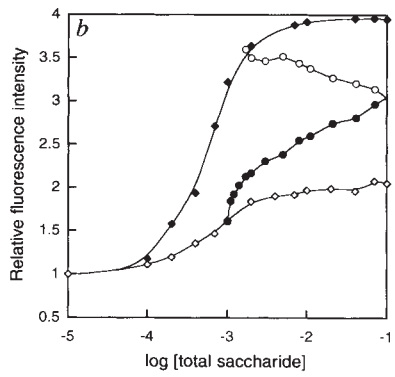

FIG. 3 *a*, Possible complexes of **3** (*R* or S) with saccharides at pH 7.77. *b*, Chiral recognition for mixtures of enantiomers. The figure shows the fluorescence intensity log [total saccharide] profile of **3***R* at 25 °C; 1.0×10^{-5} M of **3***R* in 33.3% MeOH/H_2O buffer at pH 7.77, λ_{ex} 289 nm, λ_{em} 358 nm. D-Glucose (◆); L-glucose (◇); added D-glucose from initial condition of 0.001 M L-glucose (●); added L-glucose from initial condition of 0.001 M D-glucose (○).

D-galactose (Table 1). With **3***S* the PET quenching efficiency on saccharide binding is affected most strongly by L-fructose and L-glucose; the least by D-fructose and D-glucose (Table 1). This demonstrates the electronic effects of complexation.

Previously, we demonstrated (with **2**) that the monosaccharide selectivity of a diboronic acid could be finely tuned towards one particular monosaccharide (glucose). With **3** we have now shown that selectivity towards one optical isomer of a monosaccharide can also be achieved. Furthermore, we are able to demonstrate selective recognition of one enantiomer in the presence of the other (Fig. 3*b*). We propose that the PET sensor **3** is a 'bimodal' chiral probe: both the fluorescence intensity and the stability of the 1:1 saccharide complex reflect the chirality of the bound saccharide. □

Received 25 November 1994; accepted 10 February 1995.

1. Deng, G., James, T. D. & Shinkai, S. *J. Am. chem. Soc.* **116,** 4567–4572 (1994).
2. James, T. D., Sandanayake, K. R. A. S. & Shinkai, S. *J. chem. Soc., chem. Commun.* 477–478 (1994).
3. James, T. D., Sandanayake, K. R. A. S. & Shinkai, S. *Angew. Chem.* **33,** 2207–2209 (1994).
4. Yoon, J. & Czarnik, A. W. *J. Am. chem. Soc.* **114,** 5874–5875 (1992).
5. Morin, G. T., Hughes, M. P., Paugam, M.-F. & Smith, B. D. *J. Am. chem. Soc.* **116,** 8895–8901 (1994).
6. Wulff, G. *Pure appl. Chem.* **54,** 2093–2102 (1982).
7. Rebek, J. Jr *Angew. Chem.* **29,** 245–255 (1990).
8. Goswami, S. & Hamilton, A. D. *J. Am. chem. Soc.* **111,** 3425–3426 (1989).
9. Kelly, T. R., Zhao, C. & Bridger, G. J. *J. Am. chem. Soc.* **111,** 3744–3745 (1989).
10. Etter, M. C. & Adsmond, D. A. *J. chem. Soc., chem. Commun.* 589–591 (1990).
11. Aoyama, Y., Tanaka, Y., Toi, H. & Ogoshi, H. *J. Am. chem. Soc.* **110,** 634–635 (1988).
12. Bissel, R. A. *et al. Top. Curr. Chem.* **168,** 223–264 (1993).
13. Czarnik, A. W. *Fluorescent Chemosensors for Ion and Molecular Recognition* (ACS Books, Washington DC, 1993).
14. Lorand, J. P. & Edwards, J. D. *J. org. Chem.* **24,** 769–774 (1959).
15. Irie, M., Yorozu, T. & Hayashi, K. *J. Am. chem. Soc.* **100,** 2236–2237 (1978).
16. Yorozu, T., Hayashi, K. & Irie, M. *J. Am. chem. Soc.* **103,** 5480–5484 (1981).
17. Brunner, H. & Goldbrunner, J. *Chem. Ber.* **122,** 2005–2009 (1989).
18. Bruner, H. & Wultz, K. *New J. Chem.* **16,** 57–61 (1992).
19. Brunner, H. & Schiessling, H. *Angew. Chem.* **33,** 125–126 (1994).
20. Perrin, D. D. & Dempsey, B. *Buffers for pH and Metal Ion Control* Ch. 6 (Chapman & Hall, London, 1974).
21. Fery-forgues, S., LeBris, M.-T., Guette, J.-P. & Valeur, B. *J. phys. Chem.* **92,** 6233–6237 (1988).

ACKNOWLEDGEMENTS. We thank M. Irie (Kyushu University) for helpful discussions; T.D.J. and K.R.A.S.S. thank P. Linnane and M. Mikami (JRDC Chemirecognics Project) for helpful advice; T.D.J. thanks H. Brunner for supplying detailed experimental procedures. We also thank R. Iguchi and S. Imazu for technical assistance.

Palaeoaltimetry from energy conservation principles

Chris E. Forest, Peter Molnar & Kerry A. Emanuel

Center for Meteorology and Physical Oceanography, Massachusetts Institute of Technology, Cambridge, Massachusetts 02139, USA

A KNOWLEDGE of past changes in the mean elevations of large continental areas is important for understanding both dynamic processes in the Earth's mantle[1] and the evolution of the global climate[2]. But virtually all methods for determining palaeoelevations are problematic[3], in part because changes in either elevation or climate can give rise to the same observed geological phenomena[4]. Ideally, palaeoelevations would be inferred directly from estimates of palaeopressure, and it has recently been shown[5] that vesicles in basaltic lava flows preserve a record of atmospheric pressure at the altitude of emplacement; however, the elevations thus obtained have large errors (~1.4 km), and the method can at present be applied only to lavas that have had a simple emplacement history[5]. Palaeobotanical methods for estimating palaeoelevation have received much attention[6–12], but they rely on empirical temperature–elevation relationships, the uncertainties in which are difficult to evaluate for past climates. Here we describe an alternative palaeobotanical approach, based on energy conservation in the atmosphere, in which fossil leaf assemblages are used to infer enthalpy, rather than temperature. This approach is relatively insensitive to palaeoclimate, with an expected error in palaeoelevation of ~700 m.

The use of fossil leaf assemblages for palaeoaltimetry consists of two steps: first, estimating from fossil plants a climate parameter that varies with altitude (like mean annual temperature), and second, using differences in that parameter from separate sites to estimate elevation differences[6], given *a priori* knowledge of the variation of the parameter with altitude. Mean annual temperature has been used predominantly as the climate param-

eter because it shows correlations with physiognomic characteristics of leaf samples from living plants[13–16]. Assuming that characteristics of fossil leaf assemblages obey the same relationship, palaeotemperature estimates can be inferred[7,17] with uncertainties perhaps as low as 1 °C. As mean annual temperature varies with altitude, latitude and geological time, palaeoelevation (Z) may be calculated by comparing surface temperatures, T, of high- and low-altitude locations at the same latitude and of the same age using:

$$Z = (T_{high} - T_{low})\gamma^{-1} \quad (1)$$

where $\gamma = -\partial T/\partial Z$ is the empirical relationship between mean annual temperature at the surface and altitude derived from the present climate. (Note that γ is not a gradient of T within the atmosphere and so is not a lapse rate in the meteorological sense, although it has been termed a 'terrestrial lapse rate'.)

Not only do relationships between T and Z lack a firm theoretical foundation, but large spatial variations also exist in present-day estimates of γ in the western United States[8–10]. Meyer[10] calculated local estimates of γ for 39 areas of the world with surface topography >750 m and found $\gamma = 5.9 \pm 1.1$ K km^{-1}, but with a range of 3.64–8.11 K km^{-1}. Moreover, we have no reason to expect that the present laterally varying empirical relationships should hold in the different climates that occurred in geological time. We therefore seek a measurable thermodynamic quantity whose distribution with altitude and longitude is constrained well by both theory and observations. The use of a quantity chosen to agree with fundamental thermodynamic laws is obviously more reliable than one fitted empirically to data spanning a fraction of the twentieth century—a small fraction of geological history.

Derived from the first law of thermodynamics, moist static energy[18,19], h, is the total specific energy content of air (~300 kJ kg^{-1} in mid-latitudes), excluding kinetic energy, which is very small (<5%) compared with the other terms:

$$h = c_p' T + L_v q + gZ = H + gZ \quad (2)$$

where c_p' is the specific heat capacity at constant pressure of moist air, T is temperature (in K), L_v is the latent heat of vaporization for water, q is specific humidity, g is the gravitational acceleration, Z is altitude and H is moist enthalpy. The specific heat capacity of moist air, $c_p' = (1 - q)c_{pd} + qc_{pv}$, accounts for compositional changes of the air, where c_{pd} and c_{pv} are the specific heat capacities of dry air and water vapour respectively. Although the internal energy, $c_p'T$, is the largest term in equation (2), typical variations in the three separate components are roughly of equal magnitudes, ~30–50 kJ kg^{-1}, for the ranges of T, q and Z of approximately 0–30 °C, 0–20 g kg^{-1}, and 0–4,000 m respectively.

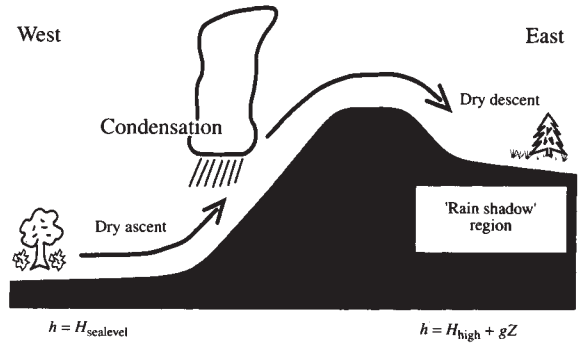

FIG. 1 Surface air conserves moist static energy as it traverses a mountainous region through conversions between sensible heat, latent heat and potential energy. During dry ascent and descent, changes in sensible heat compensate for changes in potential energy. For condensation processes at a constant height, the sensible heat increases when the latent heat of water vapour is released. The potential energy for the high-elevation site is the difference in moist enthalpy, $\Delta H = H_{sea\,level} - H_{high}$, which, via $\Delta H/g$, yields the elevation estimate.

Two properties of moist static energy make it a desirable candidate for inferring palaeoelevations. First, changed only by radiative heating and surface fluxes of latent and sensible heat, it is nearly conserved following air parcels and hence is approximately constant along trajectories. Second, the value of h in the atmospheric boundary layer (the lowest 1–1.5 km) is usually constrained by convection to be close to the value of h in the upper troposphere[20,21]. (The actual constraint is along vortex lines rather than in the vertical direction, but the difference is usually small.) The Earth's rotation causes large-scale movement in the upper troposphere to flow nearly from west to east at mid-latitudes, so that contours of h there should also trend nearly west–east. This implies that h at the surface should be nearly invariant with longitude (that is, be zonally symmetric).

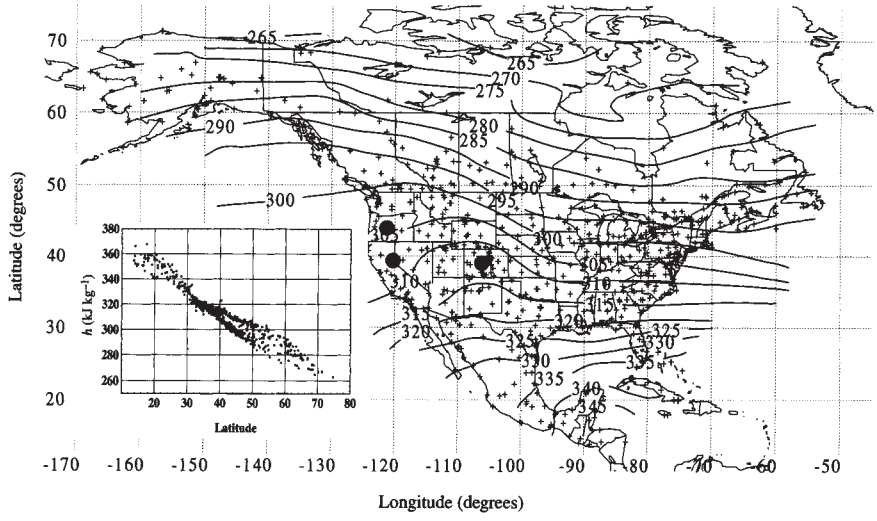

FIG. 2 The spatial distribution of mean annual moist static energy. Crosses indicate station locations from the ISMCS dataset[22]. Mean moist static energy h was calculated by independently calculating a mean temperature and mean specific humidity and by combining the respective sensible heat, latent heat and potential energies. We accounted for the temperature dependence of the latent heat of vaporization, $L_v = L_{vo} + (T - 273.15)(c_{pv} - c_l)$, where c_{pv} and c_l are the specific heat capacity at constant pressure of water vapour and liquid water, respectively, and L_{vo} is the latent heat of vaporization at 0 °C. This second-order effect and the dependence of c_p' on q are most important in warm and moist climates, where they contribute variations of ~5–10 kJ kg^{-1} corresponding to apparent differences in elevation of 500–1,000 m. Of the various averaging periods, we chose mean annual h based on the small error from zonal asymmetries and on the ability to predict mean annual enthalpy from fossil leaf physiognomy. The locations of the fossil collection sites are indicated by filled circles: Goshen, Oregon; LaPorte, California; and Florissant, Colorado. Inset, the variation of h with latitude (in degrees). Limiting the data to 30°–60° N yields the estimate of $s_h = 4.5$ kJ kg^{-1}.

As a caveat, the large-scale atmospheric flow is influenced by topography that will affect the zonal symmetry. So when applying this technique, one should ascertain the zonal symmetry of the palaeoclimate; this requires a better understanding of stationary waves in the general circulation of the atmosphere.

Assuming that h is zonally symmetric along the Earth's surface, if we can estimate enthalpy at sea level ($H_{\text{sea level}}$) for a particular latitude, it follows from equation (2) that the palaeoaltitude, Z, of another location at the same latitude is given by

$$Z=\frac{H_{\text{sea level}}-H_{\text{high}}}{g} \tag{3}$$

where H_{high} is the enthalpy at the high-altitude locations (Fig. 1). Therefore, the necessary assumptions to estimate palaeoaltitude are: (1) the surface moist static energy is zonally symmetric, and (2) the estimate of enthalpy for the regional palaeoclimate is accurate.

To examine deviations from zonal invariance of h, we examined the distribution of mean h across the North American continent (Fig. 2). Using climate data for 699 surface weather stations[22], we calculated mean h by independently calculating a mean temperature and mean specific humidity and by combining the respective sensible heat, latent heat and potential energies. We used averaging periods ranging from a season to a year, and various formulations of mean temperature and mean specific humidity. We quantified the longitudinal invariance by statistically fitting h to monotonic arbitrary functions of latitude, ϕ. Because we are testing for invariance, the standard deviation of the fit is more important than the actual latitude dependence. To minimize the expected error, we limited the data to 30°–60° N and divided them into three latitude bins of 10°. We linearly fitted the data within each band and used deviations from each to obtain a mean square error (Fig. 2). This approach reduces the expected error from zonal asymmetries of h, s_h, to 4.5 kJ kg^{-1}. Dividing s_h by g yields an estimate of the minimum error in altitude of 460 m.

We can compare this error to that deduced assuming the invariance of the terrestrial lapse rate, and therefore the longitudinal invariance of $G=T+\gamma Z$. For $\gamma=5.9$ K km^{-1} (ref. 10), we calculated deviations from longitudinal invariance of G to be 3.2 K for the present-day climate of North America. Hence a minimum standard error for estimating altitude can be computed from these results, from $s_Z^2=s_G^2/\gamma^2+((\Delta T)^2 s_\gamma^2)/\gamma^4$ where s_G and s_γ are the standard errors of G and γ respectively. With $s_\gamma=1.1$ K km^{-1} (ref. 10), minimum uncertainties in the estimated altitudes increase with altitude: $s_Z=540$ m, 660 m and 920 m for altitudes of 0 m, 2,000 m and 4,000 m, respectively. So even ignoring the unpredictable temporal changes in γ over geological time, these estimates of minimum uncertainties exceed that of 460 m from assuming longitudinal invariance in h.

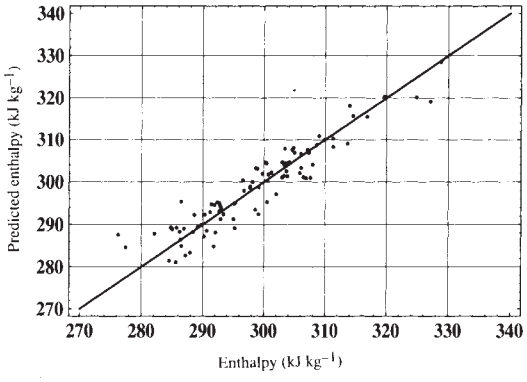

FIG. 3 The predicted mean enthalpy versus observed mean enthalpy for the annual mean, as given by equation (4) for the 92 vegetation sites (see text). The regression analysis accounts for 88% of the variations in moist enthalpy, yielding a standard error $s_H=3.9$ kJ kg^{-1}. Because humidity data are not available for each vegetation site, mean annual enthalpy for the plant collection sites is interpolated from nearby stations using the standard distance-weighted mean, $h_{\text{plant site}}=(\sum w_i h_i)/(\sum w_i)$ where $w_i=\exp(-r_i^2/d^2)$, where r_i is the radial distance from plant site to the meteorological station i, and d is the average distance to the nearest station, 90.8 km. Knowledge of the elevation, Z, and mean annual temperature, T, at the vegetation sites allows the calculation of mean moist enthalpy, $H=h-gZ$, from the interpolated value of h.

The task remains to determine mean annual enthalpy from plant physiognomy. We present results of an analysis relating foliar physiognomic characters to mean annual enthalpy that exploits the method and data developed by Wolfe[7]. We searched among an array of 29 foliar characteristic scores (p_i; see below) from 92 sites in North America for linear combinations of the foliar characteristics that covary with the local climates. At a given site, the scores are calculated as a percentage of species exhibiting each of 29 foliar characteristics: seven ranges of size, five length-to-width ratios, overall shape (obovate, elliptic, ovate, lobed), basal shape (cordate, round, acute), apical shape (emarginate, rounded, acute, attenuate), and teeth (no teeth, regular, close, round, acute, compound). We determined which foliar characteristics covary with one another (using principal components analysis) and which best correlate with enthalpy (using principal components analysis with regression[23]). This creates a predictive equation of the form:

$$H=H_0+\sum_i \alpha_i p_i \tag{4}$$

where α_i is the regression coefficient of the ith foliar characteristic. The standard error for predicting H is 3.9 kJ kg^{-1} (Fig. 3), corresponding to a minimum error in palaeoelevation of 400 m.

To illustrate the use of this method in determining palaeoelevation, we estimated H from the physiognomic characteristics for three well known fossil floral assemblages: Florissant (34.1 Myr) in central Colorado, Goshen (32 Myr) from central Oregon and LaPorte (33 Myr) from northern California (Fig. 2). Each assemblage of fossil leaves has been appropriately scored using the same characteristics as in Wolfe's data set[7] and has been used in previous estimates of Florissant's palaeoelevation including 2.3–3.3 km (refs 11, 12), 2.5 km (ref. 8) and 2.9 km (ref. 9). Using Wolfe's scores (personal communication) for the Goshen and LaPorte floras and Gregory's (ref. 11) for the Florissant flora, we calculated mean enthalpies of 294.6, 321.1 and 321.2 kJ kg^{-1}, respectively, for these assemblages. Assuming that both Goshen and LaPorte were deposited at sea level yields a sea-level value of mean enthalpy of 321.1 ± 2.8 kJ kg^{-1}. The difference in enthalpy between sea level and Florissant yields a palaeoelevation of $2{,}700\pm670$ m. Sea level 32–34 Myr ago was 180 m higher[24] than at present, so the palaeoelevation is 2.9 ± 0.7 km with respect to the present geoid. This estimate of Florissant's palaeoaltitude agrees with other recent estimates of palaeoaltitude, and therefore supports the contention of Gregory and Chase[11,12], Meyer[8] and Wolfe[9], that Florissant was high in Late Eocene/Early Oligocene time. As these workers have noted, there is a widespread belief that the Rocky Mountains were at a low elevation throughout much of the Late Cenozoic and rose early in Quaternary times. More importantly here, the 700-m uncertainty is smaller than those of other palaeoelevation estimates. □

Received 7 November 1994; accepted 17 February 1995.

1. England, P. & Houseman, G. *J. geophys. Res.* **94,** 17561–17579 (1989).
2. Raymo, M. E. & Ruddiman, W. F. *Nature* **359,** 117–122 (1992).
3. England, P. & Molnar, P. *Geology* **18,** 1173–1177 (1990).
4. Molnar, P. & England, P. *Nature* **346,** 29–34 (1990).
5. Sahagian, D. L. & Maus, J. E. *Nature* **372,** 449–451 (1994).
6. Axelrod, D. I. *Paleobotanist* **14,** 144–171 (1966).
7. Wolfe, J. A. *Bull. U.S. geol. Surv.* **2040,** (1993).
8. Meyer, H. W. thesis, Univ. California at Berkeley (1986).
9. Wolfe, J. A. *Bull. U.S. geol. Surv.* **1964** (1992).
10. Meyer, H. W. *Palaeogeogr. Palaeoclimatol. Palaeoecol.* **99,** 71–99 (1992).

11. Gregory, K. M. *Paleoclimates* (in the press).
12. Gregory, K. M. & Chase, C. G. *Geology* **20,** 581–585 (1992).
13. Bailey, I. W. & Sinnot, E. W. *Science* **41,** 831–834 (1915).
14. Bailey, I. W. & Sinnot, E. W. *Am. J. Bot.* **3,** 24–39 (1916).
15. Wolfe, J. A. & Hopkins, H. E. in *Tertiary Correlation and Climatic Changes in the Pacific* (ed. Hatai, K.) 67–76 (Sasaki, Sendai, 1967).
16. Wolfe, J. A. *Palaeogeogr. Palaeoclimatol. Palaeoecol.* **9,** 27–57 (1971).
17. Wolfe, J. A. *Prof. pap. U.S. geol. Surv.* **1106** (1979).
18. Wallace, J. M. & Hobbs, P. V. *Atmospheric Science: An Introductory Survey* (Academic, New York, 1977).
19. Emanuel, K. A. *Atmospheric Convection* (Oxford Univ. Press, New York, 1994).
20. Betts, A. K. *J. atmos. Sci.* **39,** 1484–1505 (1982).
21. Xu, K.-M. & Emanuel, K. A. *Mon. Weath. Rev.* **117,** 1471–1479 (1989).
22. International Station Meteorological Climate Summary CD-ROM Version 1.0 (Federal Climate Complex, Asheville, NC, 1990).
23. Mardia, K. V., Kent, J. T. & Bibby, J. M. *Multivariate Analysis (Academic, New York,* 1979).
24. *Haq, B. U., Hardenbol, J. & Vail, P. R. Science* **235,** 1156–1167 (1987).

ACKNOWLEDGEMENTS. We thank J. Wolfe for his contributions of data and expert advice, which made the entire plant physiognomic/climate correlations possible. We thank K. Gregory for unpublished Florissant data, A. Del Genio and K. Gregory for reviews, M. Raymo for revisions of early drafts, and R. Spicer, P. England, D. Povey and L. Stranks for discussions about palaeobotany and multivariate analysis. This work was supported by the Climate Dynamics Program in the Division of Atmospheric Sciences of the US NSF and in part by an ONR fellowship (C.E.F.).

Dorsalizing signal *Wnt*-7a required for normal polarity of D–V and A–P axes of mouse limb

Brian A. Parr & Andrew P. McMahon

Department of Molecular and Cellular Biology, Harvard University, 16 Divinity Avenue, Cambridge, Massachusetts 02138, USA

FORMATION of the vertebrate limb requires specification of cell position along three axes[1]. Proximal–distal identity is regulated by the apical ectodermal ridge (AER) at the distal tip of the growing limb[2–6]. Anterior–posterior identity is controlled by signals from the zone of polarizing activity (ZPA) within the posterior limb mesenchyme[7–9]. Dorsal–ventral identity is regulated by ectodermally derived signals[10–14]. Recent studies have begun to identify signalling molecules that may mediate these patterning activities. Members of the fibroblast growth factor (FGF) family are expressed in the AER and can mimic its proximal–distal signalling activity[15,16]. Similarly, the gene *Sonic hedgehog* (*Shh*) is expressed in the ZPA, and *Shh*-expressing cells, like ZPA cells, can cause digit duplications when transplanted to the anterior limb margin[17,18]. In contrast, no signal has yet been identified for the dorsal–ventral axis, although *Wnt*-7a is expressed in the dorsal ectoderm, suggesting that it may play such a role[19,20]. To test this possibility, we have generated mice lacking *Wnt*-7a activity. The limb mesoderm of these mice shows dorsal-to-ventral transformations of cell fate, indicating that *Wnt*-7a is a dorsalizing signal. Many mutant mice also lack posterior digits, demonstrating that *Wnt*-7a is also required for anterior–posterior patterning. We propose that normal limb development requires interactions between the signalling systems for these two axes.

Wnt-7a is expressed in the flanking ectoderm of the trunk prior to limb bud outgrowth. At 8.75 days postcoitum (d.p.c.), *Wnt*-7a expression encompasses the presumptive forelimb region, extending from the level of the last few somites into the ectoderm overlying the presomitic mesoderm (Fig. 1*a*). At the level of the presumptive hindlimb, ectodermal expression is first apparent at 9.25 d.p.c. (Fig. 1*a*). During initial stages of limb-bud outgrowth (9.25 d.p.c., forelimb; 9.75 d.p.c., hindlimb) and patterning, *Wnt*-7a transcripts are uniformly distributed throughout the dorsal limb ectoderm (Fig. 1*a*).

To investigate the function of *Wnt*-7a, we used gene targeting in mouse embryonic stem (ES) cells to generate a likely null allele (Fig. 1*b–d*). Matings between mice heterozygous for the targeted allele produced homozygous offspring at expected mendelian frequencies (+/+, 32; +/−, 70; −/−, 37). Although apparently fully viable, *Wnt*-7a$^{-/-}$ mice have limb abnormalities and are also sterile.

Ventral structures develop normally in *Wnt*-7a$^{-/-}$ limbs, but many dorsal tissues adopt ventral fates. Distal limb structures are particularly useful in distinguishing dorsal from ventral cell types (Figs 2, 3). The ventral skin of wild-type digits is devoid of fur, lacks pigmentation and exhibits a prominent set of transverse striations (Fig. 2*a*). Moreover, dermal footpads protrude at the base of the digits and at the distal tips of the digits (Fig. 2*a*). Normal flexion of the digits depends upon a specific arrangement of ventral tendons projecting to a series of small, ventrally located, sesamoid bones. In contrast, the dorsal half of the limb is pigmented, covered in hair, and does not possess footpads or sesamoid bones (Fig. 2*b*). The major dorsal tendons travel along the outside edges of the digits (Fig. 3*b*), while a larger tendon runs down the middle of the ventral surface (Fig. 3*a*). Dorsal-to-ventral transformations of mesenchyme cell fate are observed in the footpads, skin, tendons, sesamoid bones and joints of *Wnt*-7a mutant limbs.

The most striking superficial abnormalities on the dorsal surface of mutant limbs are dermal thickenings representing duplications of the footpads normally found ventrally (Fig. 2*c, e, f*). The dorsal pads are visible as early as 15.5 d.p.c. (Figs 2*g–i*, 3*d, e*) and express *Pax*-9 (Fig. 2*i*), a putative transcription factor, normally restricted to developing ventral pads (A. Neubuser and R. Balling, personal communication). Ectopic dorsal pads are pigmented, as migration of melanocytes is apparently unaffected by the *Wnt*-7a mutation.

The dorsal surfaces of the digits in severe *Wnt*-7a mutants also lose hair and acquire noticeable striations, resembling the normal ventral surface (Fig. 2*c*). The growth of nails at the dorsal–ventral interface of the digits is truncated to a variable extent (Fig. 2*c, f*), and abnormal, pigmented thickenings, which probably represent duplications of the large ventral pads found at the distal ends of the digits (Fig. 2*a*), often grow over the rudimentary nails (Fig. 2*f*).

Alterations in dorsal–ventral polarity are also apparent in the tendons and bones. In adult *Wnt*-7a mutant limbs (Fig. 3*c*), a large dorsal tendon, closely resembling the central ventral tendons (Fig. 3*a*), projects distally along each digit. These duplications of ventral tendons are clearly visible in sections through 15.5 d.p.c. mutant limbs, where the dorsal tendons appear to be mirror images of ventral tendons (compare Fig. 3*d, f* with *e, g*).

Normal flexion of the digits requires the correct arrangement of tendons and their attachment to sesamoid processes on the ventral surface of the distal limb bones. Sesamoid bones appear in their normal ventral positions in *Wnt*-7a mutants (Fig. 3*i*), but paired sesamoid processes also develop in the dorsal half of mutant paws (Fig. 3*k, n, o*). Not surprisingly, *Wnt*-7a mutant limbs show abnormal flexion due to these alterations in dorsal–ventral polarity. In contrast to the flexion of wild-type digits (Fig. 3*l*), mutant digits are generally straight (Fig. 3*n*), presumably because the duplication of ventral tendons dorsally results in similar tendons exerting counterbalancing forces on either side of the joints. In addition, the paws of mutants usually splay downwards and outwards, indicating incorrect bending at both the wrist and elbow joints (Fig. 3*p, q*).

Although we consistently observe a ventralization of the dorsal limb, the phenotype is clearly more severe distally than proximally. Interestingly, experiments in the chick indicate that ectodermal signalling only regulates dorsal–ventral patterning in the distal limb[13,14]. Thus, whereas *Wnt*-7a is important in dorsal–ventral patterning, it is likely that other mechanisms are also involved.

To determine whether changes in ectodermal cell fate contribute to the observed phenotype, we examined the expression of a number of regionally restricted ectodermal markers between 9.5 and 10.5 d.p.c. *Wnt*-7a transcripts can be detected in the dorsal ectoderm of *Wnt*-7a$^{-/-}$ limbs (data not shown), sug-